The Electronic Structure and Spectra of $[Ru(NH_3)_4(LL)]^{2+}$ (LL = bpy, bpz, bqdi) studied by Density Functional Theory and INDO/S. Charge Transfer Character of Electronic Transitions and their Solvatochromism.

S.I. Gorelsky[a,b] and A.B.P. Lever[a*]

Contribution from: [a]Department of Chemistry, York University, Toronto, Ontario M3J 1P3, Canada; [b]Department of Chemistry, Stanford University, Stanford, California 94305

Résumé

La théorie fonctionnelle de la densité et les calculs semi-empiriques ont été effectués pour une série de complexes du type $[Ru(NH_3)_4(LL)]^{2+}$ (où LL est bpy = 2,2'-bipyridine, bpz = 2,2'-bipyrazine, bqdi = o-benzoquinonediimine) pour explorer l`étendue du couplage entre les orbitals du métal et des ligands. La théorie fonctionnelle de la densité dépandante du temps et INDO/S ont été utilisés pour prévoir les spectres électroniques des complexes Les deux méthodes INDO/S et TD-DFRT révellent que les spectres électroniques des complexes $[Ru(NH_3)_4(LL)]^{2+}$ dépendent énormément sur le degré du couplage métal-ligand (LL). Le couplage électronique important entre l`atome métallique et le ligand LL conduit à la perte du comportement solvatochromique des transitions de transfert de charge métal à ligands. Les contributions des orbitales atomiques des orbitales moléculaires peuvent effectivement être utilisées pour sonder la nature des transitions électroniques et determiner leurs caractères de transfert de charge.

Abstract

Density functional theory and semiempirical calculations have been carried out on the series $[Ru(NH_3)_4(LL)]^{2+}$ (where LL is bpy = 2,2'-bipyridine, bpz = 2,2'-bipyrazine, bqdi = o-benzoquinonediimine) to explore the extent of coupling between metal and ligand orbitals. Time-dependent density-functional response theory (TD-DFRT) and INDO/S have been used to predict the electronic spectra of the complexes. Both INDO/S and TD-DFRT reveal that the electronic spectra of $[Ru(NH_3)_4(LL)]^{2+}$ depend heavily on the degree of the metal-ligand (LL) coupling. The extensive electronic coupling between the central atom and the ligand LL leads to the loss of the solvatochromic behavior of the metal-to ligand charge transfer transitions. Atomic orbital contributions to molecular orbitals can be used very effectively to probe the nature of electronic transitions and determine their charge transfer character.

Introduction

Solvatochromism refers to changes in electronic absorption spectra with solvent (1). Although most transition-metal complexes display solvatochromic behavior to some extent, the term is usually applied to species that show significant shifts (a few hundred wavenumbers or more) of absorption band energies with variation in solvent. The majority of known cases involve electronic transitions that are largely charge transfer (CT) in character.

The $[Ru(NH_3)_4(LL)]^{2+}$ complexes are interesting to study because they show different solvatochromic behavior of the metal-to-ligand charge transfer (MLCT) electronic transitions in the visible and near-

Dedicated to Professor Ian S. Butler

UV region. While the MLCT bands of $[Ru(NH_3)_4bpy]^{2+}$ display strong solvent dependence (2-8), the energies of the corresponding electronic transitions in $[Ru(NH_3)_4bqdi]^{2+}$ are not strongly affected by solvent (9).

In this paper we investigate how the metal-ligand coupling affects the energies, intensities, and solvatochromic behavior of MLCT bands of $[Ru(NH_3)_4(LL)]^{2+}$ using time-dependent density-functional response theory (TD-DFRT) (10-14) and the semiempirical INDO/S method (15-20), and how atomic orbital (AO) contributions (21) to molecular orbitals (MOs) can be used to probe the nature of electronic transitions and determine their CT character. We also demonstrate how the degree of charge transfer character in a transition and the exchange energy contribution to a transition are related to the experimental observation of solvatochromism.

Computational Methods

A combination of several computational tools is used. The complexes under consideration were initially explored at the semiempirical level and then by more sophisticated density functional calculations.

Optimized geometries at the semiempirical level were obtained using the INDO/1 method (22). HyperChem 5.11 (23) was utilized for INDO/1 and INDO/S calculations. For geometry optimizations the overlap weighting factors, f_σ and f_π, were both set at 1.00. The SCF convergence criterion was 10^{-1} cal, and geometry optimization tolerance was 5 cal Å^{-1}. The resonance parameter for $\beta_{4d}(Ru)$ of -20.0 eV (instead of -26.3 eV (22)) was used in all INDO/1 calculations (24).

DFT calculations were carried out using the Gaussian 98 program suite (25). Becke's 3-parameter hybrid functional (26) with the LYP correlation functional (27) (B3LYP) was used together with the Los Alamos effective core potential LanL2DZ (28-31). As starting geometries, the molecular structures obtained at the semiempirical INDO/1 level were used. A tight SCF convergence criterion (10^{-8} Hartree) was employed in all calculations. The stabilities of DFT wavefunctions were tested with respect to relaxing spin and symmetry constraints. Harmonic frequency calculations were performed on all the species at the level of theory of their optimization to establish the

nature of the critical point (minimum or transition point structure). The AO contributions to MOs and overlap populations were calculated using the *AOMix* program (32).

The electronic spectra of transition metal complexes were calculated with the INDO/S method using the approximation of singly excited configurations (CIS) and with TD-DFRT both on DFT (B3LYP/LanL2DZ) optimized geometries. The ruthenium and nitrogen atomic parameters of Krogh-Jespersen et al. were used (33). The overlap weighting factors, f_σ and f_π, for INDO/S calculations were set at 1.267 and 0.585 (19, 23), and the number of singly excited configurations in CIS calculations used was 1250 (25 occupied and 25 unoccupied orbitals).

It was confirmed that convergence of the calculated transition energies and oscillator strengths for transitions with energies up to 50000 cm^{-1} had been reached with the current number of the singly excited configurations. Energies and intensities of the lowest 35 singlet-singlet electronic transitions were calculated with TD-DFRT.

Since the calculated spectra usually have many absorption bands, it is difficult to judge the performance of the computational methods by just comparing the energies and oscillator strengths of absorption bands of experimental and calculated spectra.

We have chosen to calculate the absorption profiles of ruthenium complexes from a model described below. An absorption profile for a transition metal complex was calculated as a sum of Gaussian shaped bands using the formula (34):

$$\varepsilon(\omega) = 2.174*10^8 \sum_I \frac{f_I}{\Delta_{1/2}} \exp(-2.773\frac{(\omega - \omega_I)^2}{\Delta_{1/2}^2}) \quad (1)$$

where molar absorbance, ε, is given in units of mol^{-1} L cm^{-1}. The sum in Eqn. 1 includes all allowed transitions with energies, ω_I (expressed in cm^{-1}), and oscillator strengths, f_I. The total integrated intensity under an absorption profile obtained from Eqn. 1 is equal to a sum of the oscillator strengths (1):

$$4.319\times10^{-9} \int \varepsilon(\omega)d\omega = \sum_I f_I \qquad (2)$$

The Gaussian band shape was chosen because low-resolution spectroscopic bands follow this shape closely (35,36). Instead of evaluating the half-bandwidths, $\Delta_{1/2}$, for each electronic transition as suggested in Zerner's model (35), $\Delta_{1/2}$ were assumed to be equal to 3000 cm^{-1} (a typical half-bandwidth

value for the complexes under consideration). This assumption is justified because the absorption bands in the electronic spectra of the $[Ru(NH_3)_4(LL)]^{2+}$ complexes belong to the same class (MLCT transitions $Ru(4d) \rightarrow LL(\pi^*)$).

Calculations of Two-Electron Coulomb and Exchange Integrals

Calculations of two-electron Coulomb and exchange integrals (J and K respectively) (1,37) that are relevant for single-electron excitations in closed shell species were completed by using the CIS matrix eigenvalues (transition energies, ω_I) and eigenvectors, C_I, from INDO/S calculations.

Since

$$\omega = C^{-1} A \, C, \tag{3}$$

the CIS matrix A can be reconstructed by

$$A = C \, \omega \, C^{-1}, \tag{4}$$

where C is a matrix composed of the eigenvectors of A and ω is the diagonal matrix composed of the eigenvalues of A. For a single-electron excitation (α-spin or β-spin) from the occupied MO ϕ_i to the unoccupied MO ϕ_a, the diagonal matrix element of the CIS matrix is (38)

$$A_{i \rightarrow a(\alpha),\, i \rightarrow a(\alpha)} = A_{i \rightarrow a(\beta),\, i \rightarrow a(\beta)} = \varepsilon_a - \varepsilon_i - J_{ia} + K_{ia}, \tag{5}$$

and the off-diagonal element between α-spin and β-spin configurations for the same excitation $\phi_i \rightarrow \phi_a$ is

$$A_{i \rightarrow a(\alpha),\, i \rightarrow a(\beta)} = K_{ia}. \tag{6}$$

So, by knowing the CIS matrix, one can extract the necessary two-electron J and K integrals. The Coulomb and exchange integrals were derived from the Hyperchem (23) output files using the programme *SIG-JK* (39).

Results and Discussion.

The structures of the $[Ru(NH_3)_4(LL)]^{2+}$ complexes:

The optimized structure of $[Ru(NH_3)_4bpy]^{2+}$ has C_{2v} symmetry (Figure 1). Initially, the structures of $[Ru(NH_3)_4bpz]^{2+}$ and $[Ru(NH_3)_4bqdi]^{2+}$ were optimized with C_{2v} symmetry, but it turned out that such structures correspond to transition states (negative frequency vibrations were obtained corresponding to the rotation of the NH_3 ligands). The optimized energy minimum structures for the bpz and bqdi complexes in the gas phase have C_2 symmetry. However, the effective symmetry is still C_{2v}. The electronic energy differences between C_2 and C_{2v}
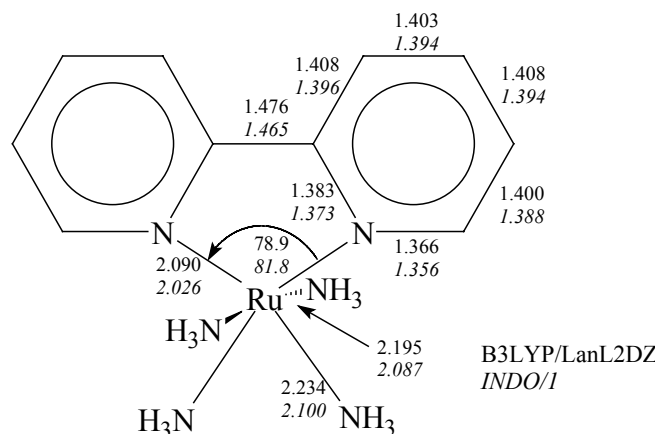

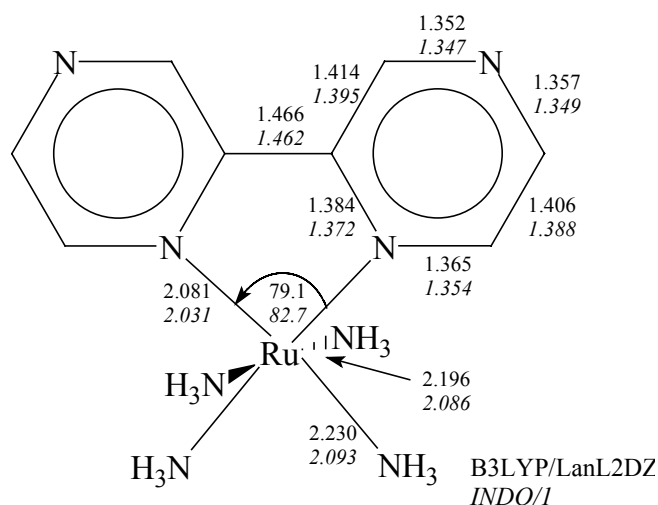Figure 1. Structure of $[Ru(NH_3)_4bpy]^{2+}$ obtained using INDO/1 and DFT (B3LYP/LanL2DZ).

Figure 2. Structure of $[Ru(NH_3)_4bpz]^{2+}$ obtained using INDO/1 and DFT (B3LYP/LanL2DZ).
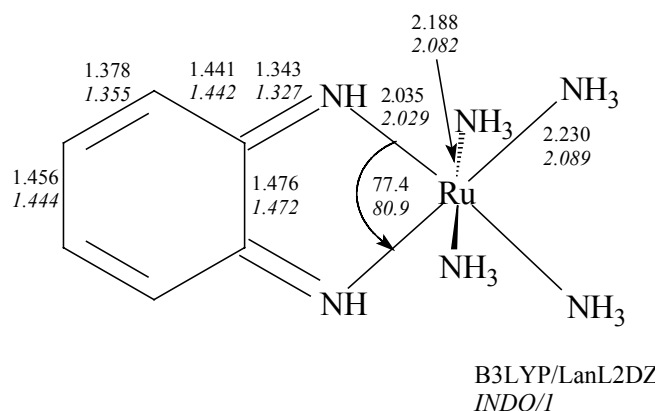

Figure 3. Structure of $[Ru(NH_3)_4bqdi]^{2+}$ obtained using INDO/1 and DFT (B3LYP/LanL2DZ).

S.I. Gorelsky and A.B.P. Lever

structures are very small (less than 5x 10^{-3} eV).

The complexes show a pseudo-octahedral arrangement of ligands (Figures 1-3) around the metal atom with axial and equatorial H_3N-Ru-NH_3 angles of 178-180º and 87-91º. The ligands LL are planar. The bqdi ligand shows the quinonoid structure with localization of the single and double C-C bonds. As expected, the Ru-N(LL) bond distances are shorter than Ru-N(H_3) distances. The short Ru-N(bqdi) distances relative to Ru-N(bpy) and Ru-N(bpz) distances reflect the much stronger metal-ligand binding when the ligand is a strong π acceptor. The equatorial (in the Ru-LL plane) Ru-N(H_3) distances are 0.007-0.013 Å (INDO/1) and 0.034-0.042 Å (B3LYP) longer than the axial Ru-N(H_3) distances. The Ru-N distances obtained with the B3LYP functional are longer than those from INDO/1 calculations and the X-ray structures of similar complexes that have (Ru-N(H_3): 2.10-2.20 Å and Ru-N(bpy): 2.03-2.10 Å) (33,40-49). The fact that the hybrid and generalized gradient approximation (GGA) exchange-correlation functionals give longer than expected Ru-N bonds can be (at least partly) attributed to the outer-sphere effects which influence the bond distances in the crystal structure but are absent in gas-phase DFT calculations (50).

Frontier Molecular Orbitals (FMOs) of [Ru(NH₃)₄(LL)]²⁺ :

With respect to the molecular orientation, the z axis coincides with the C_2 rotation axis and the ligand LL lies in the yz plane. The three highest occupied MOs of [Ru(NH₃)₄(LL)]²⁺ are mainly composed of Ru(4d) (the t_{2g} set in octahedral symmetry; all comments below concerning Ru(4d) orbitals refer to the components of this t_{2g} set). Their symmetries are a_1 + a_2 + b_1 in the C_{2v} point group. One of these orbitals (a_1) has σ-symmetry, one (b_1) has π-symmetry, and one (a_2) has δ-symmetry with respect to the LL ligand. The contribution of the ammonia ligand orbitals to these three MOs does not exceed 3%. Two electron population methods, MPA (51-55) and SCPA (56), have been applied in this paper. These methods differ in the way in which they treat electron overlap populations and converge to the same result when the overlap between AOs diminishes (21). As can be seen from Tables 1-3, there is good agreement between the two schemes for the FMOs of the [Ru(NH₃)₄(LL)]²⁺ complexes.

Free bipyridine, bipyrazine, and o-

benzoquinonediimine ligands have one low lying unoccupied π^* orbital of b_1 symmetry and two further π^* orbitals of symmetry a_2 + b_1 lying approximately 0.6-1.5 eV to higher energy.

Both DFT and INDO/S indicate that the LUMO of [Ru(NH₃)₄(LL)]²⁺ is mostly the (LL)π^* orbital with b1 symmetry. The Ru character of the LUMO of [Ru(NH₃)₄bpy]²⁺ is only 5% (B3LYP) or 3% (INDO/S) (Tables 1-3) indicating that 2,2'-bipyridine is only a moderate π-acceptor. 2,2'-Bipyrazine is a somewhat stronger π-acceptor than 2,2'-bipyridine (Table 2). The contribution of Ru orbitals to the LUMO of [Ru(NH₃)₄bpz]²⁺ is 7% (B3LYP) or 4% (INDO/S). The contribution of Ru orbitals to the LUMO of [Ru(NH₃)₄bqdi]²⁺ is 21-22% (B3LYP) or 14% (INDO/S) showing that o-benzoquinonediimine is a much stronger π-acceptor than 2,2'-bipyridine and 2,2'-bipyrazine (Table 3). Similar results were obtained by Metcalfe, Lever, and Gorelsky for [Ru(NH₃)₄(LL)]²⁺ using INDO/S and the INDO/1 optimized structures (9,57).

While the contributions of the ligand LL orbitals to the three highest filled MOs in [Ru(NH₃)₄bpy]²⁺ and [Ru(NH₃)₄bpz]²⁺ range from 3 to 18% (bpy) or from 3 to 30% (bpz); in [Ru(NH₃)₄bqdi]²⁺, they reach 47%. So, the degree of covalency in the Ru-bqdi bonding is much higher than in the bonding between Ru and the bpy and bpz ligands.

One of the three highest occupied MOs of π-symmetry is mostly Ru(4d(b_1))-localized, but does have significant ligand LL character. This is the MO which is supposedly stabilized by the π-backdonation mechanism, but it is HOMO-1 in all cases except one, [Ru(NH₃)₄bqdi]²⁺ with B3LYP/LanL2DZ, where it is HOMO-2, as might have been inferred from the Magnuson and Taube model (58).

The HOMO of the [Ru(NH₃)₄(LL)]²⁺ complexes is the Ru(4d(a_2)) orbital which also has significant ligand LL character. This orbital is stabilized through interaction with the empty LL(π^*,a_2) orbital and destabilized through interaction with a lower energy, LL π(a_2) occupied MO. The overlap populations (59) between Ru and the ligand LL are given by

$$OP_{Ru,LL}(i) = 2 \sum_{a \in Ru} \sum_{b \in LL} c_{ai} c_{bi} S_{ab} , \qquad (7)$$

where c_{ai} is the LCAO coefficient of the ath AO localized on Ru, c_{bi} is the coefficient of the bth AO localized on the ligand LL, both in the ith MO, and S_{ab} is the overlap integral for these two AOs. The

Table 1. Irreducible representations, energies, and compositions of the FMOs of [Ru(NH$_3$)$_4$bpy]$^{2+}$ (INDO/S calculation was performed on the B3LYP/LanL2DZ optimized structure).

MO	Γ	B3LYP/LanL2DZ				INDO/S			
	(C$_{2v}$)	-ε (eV)	Ru (%)[a]	bpy (%)[a]	NH$_3$ (%)[a]	-ε (eV)	Ru (%)	bpy (%)	NH$_3$ (%)
LUMO+2	a$_2$	7.34	2 / 2	98 / 98	0 / 0	6.27[b]	1	99	0
LUMO+1	b$_1$	7.51	2 / 2	97 / 96	1 / 2	5.96[b]	0	100	0
LUMO	b$_1$	8.41	5 / 5	95 / 93	0 / 2	7.16	3	97	0
HOMO	a$_2$	11.76	90 / 89	8 / 8	2 / 3	14.08	80	18	2
HOMO-1	b$_1$	11.94	85 / 85	13 / 12	2 / 3	14.15	82	16	2
HOMO-2	a$_1$	12.01	95 / 86	4 / 11	1 / 3	14.31	95	3	2
HOMO-3	a$_2$	13.23	1 / 1	99 / 99	0 / 0	14.74	7	93	0

a) AO contributions derived using MPA and SCPA respectively (32). b) The ordering of these two orbitals differs in INDO/S and DFT calculations. The numbering of MOs from INDO/S calculations was adjusted to match those from DFT calculations.

Table 2. Irreducible representations, energies, and compositions of the FMOs of [Ru(NH$_3$)$_4$bpz]$^{2+}$ (INDO/S calculation was performed on the B3LYP/LanL2DZ optimized structure).

MO	Γ	B3LYP/LanL2DZ				INDO/S			
	(C$_{2v}$)	-ε (eV)	Ru (%)[a]	bpz (%)[a]	NH$_3$ (%)[a]	-ε (eV)	Ru (%)	bpz (%)	NH$_3$ (%)
LUMO+2	b$_1$	8.30	1/ 1	98/ 97	1/ 2	6.27	0	100	0
LUMO+1	a$_2$	8.34	2/ 2	98/ 98	0/ 0	6.91	1	99	0
LUMO	b$_1$	9.32	7/ 7	92/ 91	1/ 2	7.70	4	96	0
HOMO	a$_2$	12.58	91/ 89	7/ 8	2/ 3	14.43	68	30	2
HOMO-1	b$_1$	12.78	84/ 84	13/ 12	3/ 4	14.57	83	15	2
HOMO-2	a$_1$	12.79	93/ 84	5/ 13	2/ 3	14.67	95	3	2

a) AO contributions derived using MPA and SCPA respectively (32).

Table 3. Irreducible representations, energies, and compositions of the FMOs of [Ru(NH$_3$)$_4$bqdi]$^{2+}$ (INDO/S calculation was performed on the B3LYP/LanL2DZ optimized structure).

MO	Γ	B3LYP/LanL2DZ				INDO/S			
	(C$_{2v}$)	-ε (eV)	Ru (%)[a]	bqdi (%)[a]	NH$_3$ (%)[a]	-ε (eV)	Ru (%)	bqdi (%)	NH$_3$ (%)
LUMO+1	a$_1$	7.14	67/ 47	7/ 17	26/ 36	6.16	62	7	31
LUMO	b$_1$	9.94	21/ 22	78/ 74	1/ 4	8.73	14	85	1
HOMO	a$_2$	12.28	58/ 60	41/ 37	1/ 3	14.34	52	47	1
HOMO-1	a$_1$	12.85	93/ 89	5/ 8	2/ 3	14.91[b]	93	5	2
HOMO-2	b$_1$	12.93	67/ 70	31/ 27	2/ 3	14.74[b]	68	30	2
HOMO-3	a$_2$	13.39	33/ 38	66/ 60	1/ 2	15.48	36	63	1

a) AO contributions derived using MPA and SCPA respectively (32). b) The ordering of these two MOs differs in INDO/S and DFT calculations. HOMO-2 (INDO/S) corresponds to HOMO-1 (B3LYP); HOMO-1 (INDO/S) corresponds to HOMO-2 (B3LYP). The numbering of MOs from INDO/S calculations was adjusted to match those from DFT calculations.

interaction between Ru(4d,a$_2$) and Ru(4d, b$_1$) with the unoccupied LL(π^*) levels of a$_2$ and b$_1$ symmetry generates a filled and stabilized lower lying bonding MO with positive overlap population and a higher lying (empty) MO of anti-bonding character and negative overlap population. However, as shown in Table 4, the overlap populations for the mostly Ru(4d) HOMO - 0, 1, 2 are negative. This arises because of an important anti-bonding interaction between these orbitals and filled LL(π) orbitals of appropriate symmetry. There are, of course, deeper lying, bonding interactions between Ru(4d) and LL(π) which should yield positive overlap populations; for example, the low lying a$_2$ orbital which is HOMO-3 in some complexes (see Table 4). Thus the interaction of the Ru(4d) orbitals with the occupied π orbitals of the ligand is as important as the interaction of the Ru(4d) orbitals with the unoccupied π^* (LL) orbitals. This is most clear for the [Ru(NH$_3$)$_4$bqdi]$^{2+}$ complex, where the Ru(4d,a$_2$) orbital is strongly coupled with the

Table 4. Ru-LL overlap electron populations of
$[Ru(NH_3)_4(LL)]^{2+}$ as derived from the B3LYP/LanL2DZ
calculations.

MO	LL		
	bpy	bpz	bqdi
LUMO	-0.031	-0.045	-0.095
$OP_{Ru,LL}$ [a]	**0.18**	**0.12**	**0.30**
a_2 $4d_\pi$ (δ)[b,c]	-0.053	-0.046	-0.107
b_1 $4d_\pi$ (π)[b,d]	-0.049	-0.037	-0.024
a_1 $4d_\pi$ (σ)[b,e]	-0.024	-0.023	-0.048
a_2 (π)[f]	0.002	0.002	0.036

a) Sum of the overlap populations between Ru and the ligand LL over

all occupied MOs: $OP_{Ru,LL} = \sum\limits_{i} n_i \quad OP_{Ru,LL}\,(i)$, where n_i are

the MO occupation numbers. b) Symmetry of the MO with respect to
the ligand LL. c) HOMO. d) HOMO-1 for the bpy and bpz complexes,
and HOMO-2 for the bqdi complex. e) HOMO-2 for the bpy and bpz
complexes, and HOMO-1 for the bqdi complex. f) HOMO-3 for the
bpy and bqdi complexes, and HOMO-5 for the bpz complex.

LL(π,a_2) of the bqdi ligand. This pair of orbitals forms
the HOMO and the HOMO-3 of the complex.

The sum of overlap populations over all occupied
MOs, $OP_{Ru,LL}$, (containing a Ru(4d) contribution) in
$[Ru(NH_3)_4(LL)]^{2+}$ is greater for LL = bqdi than for
LL = bpy, and LL = bpz (Table 4), implying greater
covalency in the $[Ru(NH_3)_4bqdi]^{2+}$ complex.

There have been other attempts to determine the
extent of metal-ligand mixing in $[Ru(NH_3)_4(LL)]^{2+}$.
McHale and co-workers conducted an INDO/S
calculation on $[Ru(NH_3)_4bpy]^{2+}$ using the INDO/1
optimized structure (6). According to their
calculations, the Ru contribution to the LUMO is 5%.
However, their calculated Ru characters of the
HOMO-0,1,2 (64, 66, and 88% respectively) are
underestimated (compare the corresponding values in
Table 1). The reason for this is probably an overbound
structure of the complex with very short Ru-N
distances that was obtained from the INDO/1
geometry optimization with default atomic parameters.
Hupp and co-workers applied a two-state model due to
Mulliken to probe the extent of metal-ligand orbital
mixing in $[Ru(NH_3)_4bpy]^{2+}$ (4). They found that the
electron delocalization coefficient (α_{DA}^2) is small
(0.02), as derived from the MLCT band data.
However, according an electrochemical variational
method, α_{DA}^2 is significantly higher (~0.25). Recently
Endicott et al. used a more elaborate analysis and
concluded that α_{DA}^2 is around 0.09 (8). Our results
show (Table 1, 4) that a two-state (two orbital) MLCT
model (4) provides a rather poor description of the
electronic structure of $[Ru(NH_3)_4bpy]^{2+}$. For example,
the absorbance band at 17400-20000 cm^{-1} corresponds

to several overlapping electronic transitions with
different polarization (see below).

Charge Transfer Character of Electronic Transitions:

Typically, one interprets features in the electronic
spectra of transition metal complexes as d-d, MLCT,
ligand-to-metal charge transfer (LMCT), or intra-
ligand transitions (1). However, such descriptions are
only appropriate in the weak metal-ligand coupling
limit, where "pure" CT excited states are most
rigorously defined. When the metal-ligand coupling is
high, the MOs are of mixed metal-ligand character,
and descriptions of electronic transitions such as *pure*
d-d, MLCT, LMCT, or intra-ligand become
approximate.

For characterization of the electronic transitions as
partial CT transitions the following definition of the
CT character can be used (60):

$$CT_I\,(\%) = 100\,(P_g(M) - P_I(M)), \qquad (\mathbf{8})$$

where $P_g(M)$ and $P_I(M)$ are electronic densities on the
metal in the electronic ground and excited states,
respectively. Positive CT_I values correspond to MLCT
transitions; negative CT_I values correspond to LMCT
transitions.

This definition can be re-written using the AO
contributions to MOs. Then, the CT character for the
HOMO-x→LUMO+y excitation is:

$$CT\,(\%) = \%(Ru)_{HOMO-x} - \%(Ru)_{LUMO+y}\,. \quad (\mathbf{9})$$

If the excited state is formed by more than one
single-electron excitation, then the CT character of
this excited state is expressed as a sum of CT
characters of each participating excitation, $\phi_i \rightarrow \phi_a$:

$$CT_I\,(\%) = \sum\limits_{i,a}\,[C_I(i \rightarrow a)]^2\,(\,\%(Ru)_i - \%(Ru)_a\,), \quad (\mathbf{10})$$

where CI ($i \rightarrow a$) are the corresponding coefficients of
the *I*-th eigenvector of the CIS matrix. So, one can use
the AO contributions to MOs to probe the nature of
electronic transitions.

Electronic Spectra of $[Ru(NH_3)_4(LL)]^{2+}$

$[Ru(NH_3)_4bpy]^{2+}$

The spectrum of the complex (Figure 4) in CH_3CN
consists of one band at 19200 cm^{-1} ($\varepsilon = 4.0 \times 10^3$ mol[-1]
L cm^{-1}, $f = 0.048$), a stronger band at 27200 cm^{-1} ($\varepsilon =
6.4 \times 10^3$ mol[-1] L cm^{-1}, $f = 0.11$), and another band at
33900 cm^{-1} ($\varepsilon = 3.3 \times 10^4$ mol[-1] L cm^{-1}) (2-8). The
observed lowest energy transition shows strong
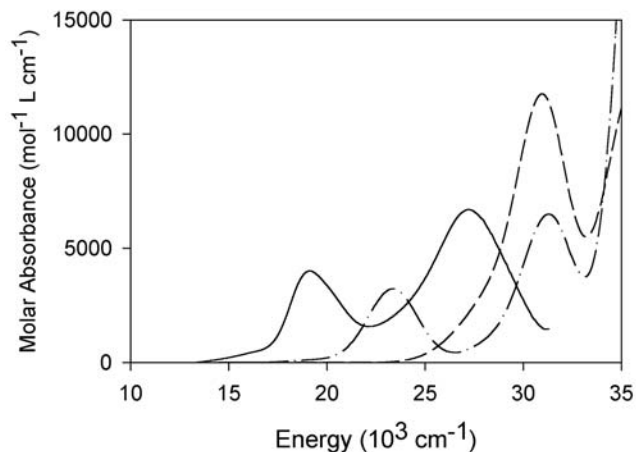solvatochromic behavior and shifts to lower energy as

Figure 4. Experimental (solid line) and simulated (TD-DFRT, dot-dash line; INDO/S, hatched line) electronic spectra of [Ru(NH₃)₄bpy]²⁺. The experimental spectrum is taken in water at 298 K (8). The intensities of electronic transitions from INDO/S calculations are reduced by a factor of 2.

the donor number of the solvent is increased (19600 cm⁻¹ in CH₃NO₂ to 17400 cm⁻¹ in hexamethylphosphoramide) (2), in accord with its assignment as an MLCT transition (and being due to solvent- H-N hydrogen bonding). The electro-optical absorption data for the complex were obtained by Hug and Boxer (5). Their data show that the dipole moment changes during the optical transitions are 6 ± 1, 6 ± 1, and 3.1 ± 0.5 D for the three bands. So, the transitions at 19200 cm⁻¹ and at 27200 cm⁻¹ were assigned to MLCT transitions from the 4d(Ru) orbitals to LUMO and LUMO+1 localized on the bpy ligand. Bipyridine complexes usually exhibit (1) two d → π* MLCT bands separated by about 8000 cm⁻¹. A smaller dipole change observed for the near-UV transition at 33900 cm⁻¹ suggested a mixing between MLCT and intra-ligand excitations for this band.

Sizova and co-workers (61-64) and Streiff et al. (6) have studied this system using CINDO/S and INDO/S respectively. Streiff et al. also used a model with point

charges to model the solvatochromic shifts. Putting four negative charges (-0.5 a.u.) 2.8 Å from the ammonia ligands of the complex resulted in a 4000 cm⁻¹ red shift of the $b_1 \rightarrow b_1$ MLCT transition.

According to TD-DFRT and INDO/S calculations, the lowest energy transition corresponds to the MLCT transition, HOMO (a_2)→LUMO (b_1) (Table 5). However, the calculated intensity of this transition is too low to correspond (on its own) to the first experimentally observed band at 19200 cm⁻¹ (f = 0.048). The stronger MLCT transition, HOMO-1(b_1)→LUMO (b_1), should be assigned to this band. Note that oscillator strengths from INDO/S calculations are usually twice as high as those from TD-DFRT calculations. However, gas-phase TD-DFRT and INDO/S calculations, by failing to take solvent effects into account, overestimate the transition energy of the strong MLCT band by 4000 cm⁻¹ and 8000 cm⁻¹ respectively. This is not surprising considering the high CT character of this band (79-82%) and its solvatochromism.

The band at 27200 cm⁻¹ (f = 0.11) is another MLCT transition expected to involve LUMO+1. According to TD-DFRT calculations it corresponds to a transition to the excited state formed by mixing the HOMO-1(b_1)→LUMO+1(b_1) and HOMO(a_2)→LUMO+2(a_2) excitations. There is no other MLCT transition with an oscillator strength as high as 0.1.

The intense absorption band at 33900 cm⁻¹ corresponds to a ligand-centered transition. Its assignment is the same according to both methods, namely HOMO-3 (a_2)→LUMO (b_1).
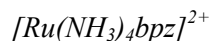
[Ru(NH₃)₄bpz]²⁺

This complex has not been prepared and so there are no experimental spectroscopic data for it. The calculated spectrum (Table 6, Figure 5) of the complex closely resembles that of [Ru(NH₃)₄bpy]²⁺. The three

Table 5. Comparison between experimental and calculated electronic spectra (10^3 cm⁻¹) of [Ru(NH₃)₄bpy]²

Expt.	TD-DFRT (B3LYP/LanL2DZ)			INDO/S		
ω_l, f [a]	ω_l	F	Assignment	ω_l	F	Assignment
	19.5	0.0016	H→L (96%)	26.3	0.011	H→L (94%)
	21.1	0.0000	H-2→L (97%)	27.7	0.0001	H-2→L (73%)
19.2 (f=0.048)	23.4	0.045	H-1→L (84%)	27.8	0.032	H-1→L (55%)
				28.8	0.040	H-2→L+3 (55%)
27.2 (f=0.11)	31.4	0.079	H-1→L+1 (42%),	35.1	0.21	H→L+2 (54%)
			H→L+2 (41%)	36.4	0.17	H-1→L+2 (92%)
33.9	36.4	0.46	H-3→L (67%)	31.0	0.31	H-3→L (82%)

a) The experimental spectrum in CH₃CN at 298 K (8). H = HOMO, L = LUMO

Table 6. Calculated electronic spectrum of $[Ru(NH_3)_4bpz]^{2+}$.

TD-DFRT (B3LYP/LanL2DZ)			INDO/S		
ω_l	f	Assignment	ω_l	f	Assignment
18.2	0.0022	H→L (96%)	23.8	0.030	H→L (85%)
19.5	0.0001	H-2→L (96%)	25.7	0.0008	H-2→L (91%)
23.4	0.035	H-1→L (75%)	26.8	0.038	H-1→L (74%)
35.1	0.45	H-5[a]→L (66%)	28.7	0.39	H-3[a]→L (88%)

a) The relative ordering of these orbitals differs in INDO/S and DFT calculations.
HOMO-3 (INDO/S) corresponds to HOMO-5 (B3LYP).

Table 7. Comparison between experimental and calculated electronic spectra of $[Ru(NH_3)_4bqdi]^{2+}$.

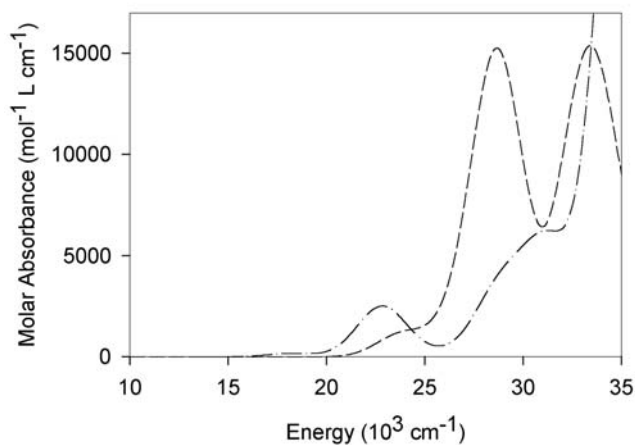| Expt. ω_l[a]	TD-DFRT (B3LYP/LanL2DZ)			INDO/S		
	ω_l	f	Assignment	ω_l	f	Assignment
10.4	10.4	0.0007	H→L (75%)	13.4	0.015	H→L (93%)
	12.9	0.0000	H-1→L (92%)	15.7	0.0000	H-1→L (97%)
	21.5	0.014	H-3→L (82%)	22.8	0.042	H-3→L (93%)
21.3 (f= 0.17)	23.4	0.22	H-2→L (64%)	22.4	0.41	H-2→L (91%)

a) The experimental spectrum in CH_3CN at 298 K (9).

Figure 5. Simulated (TD-DFRT, dot-dashed line; INDO/S, hatched line) electronic spectra of $[Ru(NH_3)_4bpz]^{2+}$. The intensities of electronic transitions from INDO/S calculations are reduced by a factor of 2.

Figure 6. Experimental (solid line) and simulated (TD-DFRT, dot-dashed line and INDO/S, hatched line) electronic spectra of $[Ru(NH_3)_4bqdi]^{2+}$. The experimental spectrum is taken in water at 298 K.[9] The intensities of electronic transitions from INDO/S calculations are reduced by a factor of 2.

lowest energy transitions correspond to the MLCT transitions from 4d(Ru) to the LUMO (b_1) which is localized on the bipyrazine ligand. The strongest among them corresponds to HOMO-1 (b_1)→LUMO (b_1).

[Ru(NH₃)₄bqdi]²⁺

Table 7 and Figure 6 show a comparison between the observed (9) and the calculated spectra of $[Ru(NH_3)_4bqdi]^{2+}$. Unlike $[Ru(NH_3)_4bpy]^{2+}$, where the calculated MLCT transition energies are significantly higher than the observed ones, both TD-DFRT and INDO/S reproduce the experimental spectrum of the
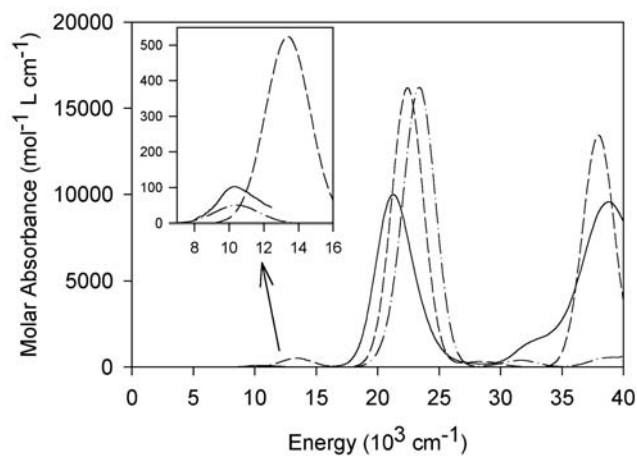
$[Ru(NH_3)_4bqdi]^{2+}$ complex very well, although the INDO/S predicted intensities are at least twice those observed.

The principal visible-region absorption band at 21300 cm^{-1} (f = 0.17) is due to the transition from the Ru(4d, b_1) to the bqdi ligand π^* orbital, i.e. HOMO-2 (b_1)→LUMO (b_1). This can be described as an MLCT transition, but there is significant $\pi \rightarrow \pi^*$ character as can be seen from Table 3.

According to TD-DFRT and INDO/S, the weaker HOMO-3 → LUMO transition is hidden in the principal HOMO-2 → LUMO band. Its intensity is
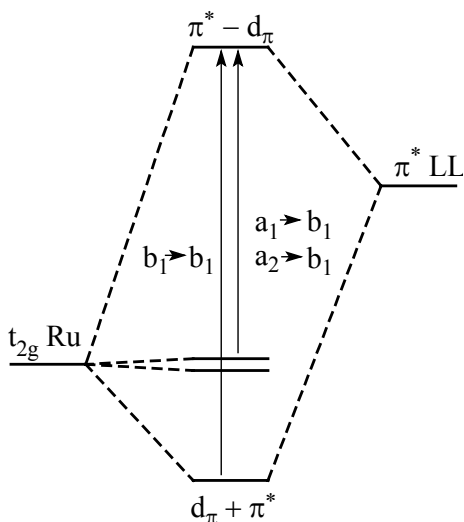
Figure 7. Magnuson and Taube model showing one d_π orbital stabilized relative to the other two d_π orbitals by π-backdonation to the ligand π^* level.

Table 8. Orbital energy splitting of the Ru d_π sub-shell, Δd_π, and the calculated energy separation between the $a_2 \rightarrow b_1$ and $b_1 \rightarrow b_1$ MLCT transition, $\Delta \omega_{MLCT}$, for [Ru(NH₃)₄(LL)]²⁺ (all quantities are in 10^3 cm⁻¹).

LL	INDO/S		B3LYP/LanL2DZ	
	Δd_π	$\Delta \omega_{MLCT}$	Δd_π	$\Delta \omega_{MLCT}$
bpy	1.8	1.5	2.0	3.9
bpz	1.9	3.0	1.7	5.2
bqdi	4.6	9.1	5.2	13.0

6 - 10% of the principal transition and is mostly a $\pi \rightarrow \pi^*$ transition but with some MLCT contribution.

The lowest energy electronic transition from Ru(4d,a_2), HOMO (a_2)→LUMO (b_1), appears as a weak near-infrared absorption (Figure 6, insert). There is one more possible MLCT transition, namely Ru(4d,a_1) $\rightarrow \pi^*$(bqdi); this is HOMO-1 (a_1)→LUMO (b_1). However, its calculated intensity is very weak, and it is not identified in the spectrum of [Ru(NH₃)₄bqdi]²⁺. The appearance of the low-energy MLCT transitions is further discussed below. The energy spanned by the three lowest energy MLCT transitions (TD-DFRT: 13000 cm⁻¹; INDO/S: 9100 cm⁻¹) is much higher than the corresponding spread in [Ru(NH₃)₄(LL)]²⁺ with LL=bpy and bpz, a sign of stronger metal-ligand coupling in the [Ru(NH₃)₄bqdi]²⁺ complex.

The stronger electronic coupling, or greater covalency, in the bqdi complex leads to the increased intensity (1) of the principal MLCT transition compared to the [Ru(NH₃)₄(LL)]²⁺ with bpy and bpz

ligands. The experimental and calculated oscillator strength of this transition in the bqdi complex are 5-6 times higher than those in the bpy and bpz complexes. This transition gains significant $\pi \rightarrow \pi^*$ character in [Ru(NH₃)₄bqdi]²⁺. Indeed, while in [Ru(NH₃)₄bpy]²⁺ the HOMO-1 (b_1)→LUMO (b_1) band has ~80% MLCT character, the similar band in [Ru(NH₃)₄bqdi]²⁺, HOMO-2 (b_1)→LUMO (b_1), has only ~50% MLCT character. So, the net change in dipole moment between ground and excited state decreases, and the formal MLCT transition loses its characteristic solvatochromic behavior. This is the reason why gas-phase TD-DFRT and INDO/S calculations reproduce the electronic spectrum of the [Ru(NH₃)₄bqdi]²⁺ complex in solution accurately and perform very differently when dealing with the electronic spectrum of [Ru(NH₃)₄bpy]²⁺.

Low Energy Weak MLCT Transitions and Magnuson-Taube Analysis:

As shown above, in addition to the strong MLCT transitions there are low-energy weak MLCT transitions which are observed in the electronic spectrum of [Ru(NH₃)₄bqdi]²⁺. An explanation of the two MLCT transitions has been given by various authors, but in the first instance by Magnuson and Taube (58).

In the general species [Ru(NH₃)₄(LL)]²⁺, only one occupied Ru(4d) orbital has the proper symmetry (b_1) to interact with the LUMO of the ligand LL leading to bonding and anti-bonding combinations (Figure 7). To first order, the other two Ru(4d) orbitals will not be stabilized, and so transitions from these two Ru(4d) orbitals to the LUMO should occur to the red of the main visible region band. However, they will be very weak due to poor ground-excited state overlap and are usually obscured by the strong band, except when they are displaced to very low energy (as in the bqdi complex).

Both INDO/S and TD-DFRT reveal that the two weak MLCT bands are indeed well separated (to lower energy) from the Ru(4d,b_1) →LL (π^*, b_1) transition in [Ru(NH₃)₄bqdi]²⁺, while for [Ru(NH₃)₄(LL)]²⁺ (LL= bpy, bpz), these weak transitions are calculated to lie close to the main visible region band. The separation between these weak bands and the main absorption band increases with increasing π^*-acceptor character of the ligand, i.e. with increasing Ru - LL mixing (Table 8), e.g. also see ref. 65. However, the overall

Table 9. Molecular Coulomb J(HOMO-x, LUMO) and exchange K(HOMO-x, LUMO) integrals for $[Ru(NH_3)_4(LL)]^{2+}$ (INDO/S calculations, all quantities are in 10^3 cm^{-1}).

LL	J (HOMO-x, LUMO)			K (HOMO-x, LUMO)		
	x=0	x=1	x=2	x=0	x=1	x=2
	(δ)[a]	(π)	(σ)	(δ)	(π)	(σ)
bpy	31.0	30.5	29.2	1.1	2.0	0.1
bpz	32.7	31.2	30.2	1.6	2.4	0.2
bqdi	37.6	37.3	34.7	3.7	7.2	0.7

a) Symmetry of the MO with respect to the ligand LL

splitting of the Ru(4d) sub-shell (as illustrated in Figure 7) is significantly smaller than any of the corresponding energy separations between strong and weak MLCT bands (Table 8). So, the Magnuson and Taube model (58), taking only the orbital energy differences into account, is incomplete. As was suggested by Shin and co-workers (66) for the $[Ru(NH_3)_5(L)]^{2+}$ complexes and by ourselves (24,57) for the $[Ru(LL)_n(bpy)_{3-n}]^{2+}$ complexes (LL= abpy, bpz, bqdi), another major cause of the transition energy differences between the strong and weak MLCT bands is varying Coulomb and exchange contributions.

Coulomb and Exchange Contributions to MLCT Transition Energies:

In the absence of configuration interaction, the energies for the first three MLCT transitions in $[Ru(NH_3)_5(LL)]^{2+}$ are given by (67):

$$\omega_x = \varepsilon_{LUMO} - \varepsilon_{HOMO-x} - J\text{ (HOMO-x, LUMO)}$$
$$+ 2K\text{ (HOMO-x, LUMO)}, \qquad \textbf{(11)}$$

where ε is the MO energy, J is the Coulomb integral, and K is the exchange integral. The quantity $(-J + 2K)$ is negative and usually quite large for the Hartree-Fock (HF) and HF-like methods, so that the transition energy ω_x is significantly less in energy than the HOMO - LUMO gap. In view of the comparative data discussed above, it is evident that the $(-J + 2K)$ term must be very different for the weak and strong MLCT transitions. Table 9 lists the J and K values as calculated by the INDO/S method for the $[Ru(NH_3)_4(LL)]^{2+}$ complexes.

For $[Ru(NH_3)_4bqdi]^{2+}$, HOMO-2(b_1) $\rightarrow$ LUMO(b_1) is a transition between two MOs which are formed from mixing the same AOs. There is, therefore, little net CT, as experimentally confirmed by the lack of solvatochromism for $[Ru(NH_3)_4bqdi]^{2+}$. Thus, the center of the charge distribution in the corresponding excited state is very close to that in the ground state, and K, which depends inversely on the exponential of the donor-acceptor separation, is large for the π-type transition. The K values for the σ- and δ-type

bands are lower than for the π-type (Table 9).

The Coulomb integrals depend inversely on the donor-acceptor separation. Thus, the J values also increase with increasing metal-ligand coupling, but they are less sensitive to metal-ligand coupling than are the exchange integrals. The J values for the σ- and δ-type MLCT bands are lower than for the π-type.

The energy difference between the Ru(4d,b_1) $\rightarrow$ LL (π^*, b_1) transition and lower-energy MLCT transitions then becomes an indicator of extensive mixing not solely because of the dπ splitting, though this plays a role, but because the principal transition is shifted to the blue relative to other MLCT transition by a larger exchange contribution. This is seen in the data presented in Table 9, where consideration of the magnitudes of K and to a lesser degree J leads to a more detailed understanding of the spectra of $[Ru(NH_3)_4(LL)]^{2+}$. For the Ru(4d,b_1) $\rightarrow$ LL (π^*, b_1) transition, K is relatively small (2000 cm^{-1}) for $[Ru(NH_3)_4bpy]^{2+}$ and increases to 7200 cm^{-1} for the highly coupled bqdi species. This provides a quantitative view of our contention of increasing coupling from bpy < bpz < bqdi.

In the case of the weak, low energy Ru(4d,a_2) $\rightarrow$ LL (π^*, b_1) transition (HOMO $\rightarrow$ LUMO), the donor Ru(4d, a_2) is not coupled to LL (π^*, b_1) so that there is a greater degree of charge redistribution; the charge in the excited state is spread over more of the ligand and K is smaller (Table 9). By the same argument, the Coulomb term in this transition is slightly smaller than in the Ru(4d,b_1) $\rightarrow$ LL (π^*, b_1) transition. Thus the term $(-J + 2K)$ in Eqn. 11 is significantly more negative in the Ru(4d,a_2) $\rightarrow$ LL (π^*, b_1) transition than in the Ru(4d,b_1) $\rightarrow$ LL (π^*, b_1) transition. This is the primary reason for the red shift of the weak transition relative to the strong MLCT transition.

Conclusions

The electronic structure and spectra calculations for $[Ru(NH_3)_4(LL)]^{2+}$ using INDO/S and TD-DFRT (B3LYP) show good agreement between the two methods, in spite of the large conceptual differences between these methodologies for obtaining electronic spectra.

Both INDO/S and TD-DFRT reveal that the electronic spectra of $[Ru(NH_3)_4(LL)]^{2+}$ depend heavily on the degree of the metal-ligand (LL) coupling. For

the complexes with weak coupling (such as $[Ru(NH_3)_4bpy]^{2+}$), the spread in the Ru(4d)$\rightarrow$ LL (π^*) MLCT transition energies is small. For the complexes with strong coupling (such as $[Ru(NH_3)_4bqdi]^{2+}$), the spread is large. In this complex, the strong and weak MLCT bands are well separated due to differences in the orbital energies and exchange contributions *K*, and this separation increases with increasing Ru(4d) – ligand LL mixing. In these types of complex, the presence of a weak low-energy MLCT band may serve as an indicator of significant covalency of metal-ligand bonds.

The extensive electronic coupling between the central atom and the ligand LL can lead to the loss of the solvatochromic behavior of the MLCT bands, as has been demonstrated. For the $[Ru(NH_3)_4bqdi]^{2+}$ complex, which shows little solvatochromism, TD-DFRT calculations with the B3LYP functional reproduce all features of the experimental electronic spectra and predict the transition energies and intensities accurately. INDO/S calculations are less accurate when predicting the intensities of electronic transitions. For the $[Ru(NH_3)_4bpy]^{2+}$ complex, which shows strong solvatochromism, the MLCT energies from gas-phase TD-DFRT and INDO/S calculations are significantly blue-shifted relative to experiment, because solvent stabilization of the MLCT excited state has not been taken into account.

The calculation of an absorption profile as a sum of Gaussian shaped bands appears to be a useful and simple procedure to estimate low-resolution absorption spectra of transition metal complexes.

Supporting Information

Please visit our web site shown below for CHIME readable xyz coordinate files for the optimized structures and files with a more detailed listing of the predicted electronic spectra and MO data. http://www.chem.yorku.ca/profs/lever and click on "Publications".

Acknowledgements

References

1. Lever, A. B. P. *Inorganic Electronic Spectroscopy*, 2nd ed.; Elsevier: Amsterdam, 1984.
2. Curtis, J. C.; Sullivan, B. P.; Meyer, T. J. *Inorg. Chem*., **22**, 224 (1983).
3. Doorn, S. K.; Hupp, J. T. *J. Am. Chem. Soc*., **111**, 4704 (1989).
4. Mines, G. A.; Roberts, J. A.; Hupp, J. T. *Inorg. Chem*., **31**, 125 (1992).
5. Hug, S. J.; Boxer, S. G. *Inorg. Chim. Acta*, **242**, 323 (1996).
6. Streiff, J. H.; Edwards, W. D.; McHale, J. L. *Chem. Phys. Lett*., **312**, 369 (1999).
7. Streiff, J. H.; Edwards, W. D.; McHale, J. L. *J. Chem. Phys.*, **112**, 841 (2000).
8. Endicott, J. F.; Schlegel, H. B.; Uddin, Md. J.; Seniveratne, D. S. *Coord. Chem. Rev*., **229**, 95 (2002).
9. Metcalfe, R. A.; Lever, A. B. P. *Inorg. Chem*., **36**, 4762 (1997).
10. Casida, M. E. *Time-Dependent Density Functional Response Theory of Molecular Systems: Theory, Computional Methods and Functionals*, Seminario, J. M., Ed.; Elsevier Science B. V.: Amsterdam, Theoretical and Computational Chemistry, 1995; pp 391-439.
11. Casida, M. E. In *Recent Advances in Density Functional Methods*; Chong, D. P. Ed.; World Scientific: Singapore, 1995; Chapter 5, pp155-192.
12. Gross, E. K. U.; Dobson, J. F.; Petersilka, M. *Density Functional Theory of Time-Dependent Phenomena*; Nalewalski, R. F., Ed.; Springer: Berlin, Topics in Current Chemistry, 1996; pp 81-172.
13. Stratmann, R. E.; Scuseria, G. E.; Frisch, M. J. *J. Chem. Phys*., **109**, 8218 (1998).
14. Koch, W.; Holthausen, M. C. *A Chemist's Guide to Density Functional Theory*, 2nd ed.; Wiley-VCH: Weinheim, 2001.
15. Ridley, J.; Zerner, M. C. *Theor. Chim. Acta*, **32**, 111 (1973).
16. Ridley, J. E.; Zerner, M. C. *Theor. Chim. Acta*, **42**, 223 (1976).

17. Bacon, A. D.; Zerner, M. C. *Theor. Chim. Acta*, **53**, 21 (1979).

18. Zerner, M. C.; Loew, G. H.; Kirchner, R. F.; Mueller-Westerhoff, U. T. *J. Am. Chem. Soc.*, **102**, 589 (1980).

19. Zerner, M. C. Semiempirical Molecular Orbital Methods. In *Reviews In Computational Chemistry*; Lipkowitz, K. B., Boyd, D. B., Eds.; VCH Publishers: New York, 1991; Vol. 2, Chapter 8, pp 313-365.

20. Martin, C. H.; Zerner, M. C. Electronic Structure Calculations on Transition Metal Complexes: *Ab-Initio* and Approximate Models. In *Electronic Structure and Spectroscopy of Inorganic Compounds*, Solomon, E. I., Lever, A. B. P., Eds.; John Wiley & Sons: New York, 1999; Vol. 1, Chapter 10, pp 555-659.

21. Gorelsky, S. I.; Lever, A. B. P. *J. Organomet. Chem.*, **635**, 187 (2001).

22. Anderson, W. P.; Cundari, T. R.; Zerner, M. C. *Int. J. Quantum Chem.*, **39**, 31 (1991).

23. HyperChem for Windows, Release 5.11 Professional Version, Hypercube Inc., Gainesville, Florida, USA, 1997.

24. Gorelsky, S. I.; Dodsworth, E. S.; Lever, A. B. P.; Vlcek, A. A. *Coord. Chem. Rev.*, **174**, 469 (1998).

25. Frisch, M. J.; Trucks, G. W.; Schlegel, H. B.; Scuseria, G. E.; Robb, M. A.; Cheeseman, J. R.; Zakrzewski, V.G.; Montgomery, J.A.Jr.; Stratmann, R. E.; Burant, J. C.; Dapprich, S.; Millam, J. M.; Daniels, A. D.; Kudin, K. N.; Strain, M. C.; Farkas, O.; Tomasi, J.; Barone, V.; Cossi, M.; Cammi, R.; Mennucci, B.; Pomelli, C.; Adamo, C.; Clifford, S.; Ochterski, J.; Petersson, G. A.; Ayala, P.Y.; Cui, Q.; Morokuma, K.; Malick, D. K.; Rabuck, A. D.; Raghavachari, K.; Foresman, J. B.; Cioslowski, J.; Ortiz, J. V.; Stefanov, B. B.; Liu, G.; Liashenko, A.; Piskorz, P.; Komaromi, I.; Gomperts, R.; Martin, R. L.; Fox, D. J.; Keith, T.; Al-Laham, M. A.; Peng, C. Y.; Nanayakkara, A.; Gonzalez, C.; Challacombe, M.; Gill, P. M. W.; Johnson, B.; Chen, W.; Wong, M. W.; Andres, J. L.; Gonzalez, C.; Head-Gordon, M.; Replogle, E. S.; Pople, J. A. Gaussian 98, Revision A.7, Gaussian, Inc., Pittsburgh PA, 1998.

26. Becke, A. D. *J. Chem. Phys.*, **98**, 5648 (1993).

27. Lee, C.; Yang, W.; Parr, R. G. *Phys. Rev.*, **B37**, 785 (1988).

28. Hay, P. J.; Wadt, W. R. *J. Chem. Phys.*, **82**, 270 (1985).

29. Hay, P. J.; Wadt, W. R. *J. Chem. Phys.*, **82**, 284 (1985).

30. Hay, P. J.; Wadt, W. R. *J. Chem. Phys.*, **82**, 299 (1985).

31. Dunning, T. H.; Hay, P. J. In *Modern Theoretical Chemistry*. Schaefer III, H. F., Ed.; Plenum: New York, 1976; Vol. 3, p.1.

32. Gorelsky, S. I.; *AOMix* program, http://www.obbligato.com/software/aomix/.

33. Krogh-Jespersen, K.; Westbrook, J. D.; Potenza, J. A.; Schugar, H. J. *J. Am. Chem. Soc.*, **109**, 7025 (1987).

34. Gorelsky, S. I.; *SWizard* program, http://www.obbligato.com/software/swizard/.

35. Pearl, G. M.; Zerner, M. C.; Broo, A.; McKelvey, J. *J. Comput. Chem.*, **19**, 781 (1998).

36. Endicott, J. F. In *Electron Transfer in Chemistry*; Balzani, V. Ed.; Wiley-VCH: Weinheim, 2001; Vol. 1, Chapter 7, pp.238-270.

37. Szabo, A.; Ostlund, N. S. *Modern Quantum Chemistry*; Dover Publications: Mineola, NY, 1996.

38. Dunning, T. H.; McKoy, V. J. Chem. Phys., **47**, 1735 (1967).

39. Gorelsky, S. I.; *SIG-JK* program, http://www.obbligato.com/software/sig-jk/.

40. Stynes, H. C.; Ibers, J. A. *Inorg. Chem.*, **10**, 2304 (1971).

41. Wishart, J. F.; Bino, A.; Taube, H. *Inorg. Chem.*, **25**, 3318 (1986).

42. Hambley, T. W.; Lay, P. *Inorg. Chem.*, **25**, 4553 (1986).

43. Crutchley, R. J.; McCaw, K.; Lee, F. L.; Gabe, E. J. *Inorg. Chem.*, **29**, 2576 (1990).

44. Chou, M. H.; Szalda, D. J.; Creutz, C.; Sutin, N. *Inorg. Chem.*, **33**, 1674 (1994).

45. Shin, Y.-g. K.; Szalda, D. J.; Brunschwig, B. S.; Creutz, C.; Sutin, N. *Inorg. Chem.*, **36**, 3190 (1997).

46. Bottomley, F. *J. Chem. Soc., Dalton Trans.*, 1600 (1974).

47. Rillema, D. P.; Jones, D. S. *J. Chem. Soc., Chem. Commun.*, 849 (1979).

48. Biner, M.; Bürgi, H.-B.; Ludi, A.; Röhr, C. *J. Am. Chem. Soc.*, **114**, 5197 (1992).

49. Tamura, H.; Ikeda, N.; Iguro, T.; Ohno, T.;

Matsubayashi, G.-E. *Acta Cryst.*, **C52**, 1394 (1996).

50. Broo, A. *Int. J. Quantum Chem., Quantum Chem. Symp.*, **30**, 1331 (1996).
51. Mulliken, R.S. *J. Chem. Phys.*, **23**, 1833 (1955).
52. Mulliken, R.S. *J. Chem. Phys.*, **23**, 1841 (1955).
53. Mulliken, R.S. *J. Chem. Phys.*, **23**, 2338 (1955).
54. Mulliken, R.S. *J. Chem. Phys.*, **23**, 2343 (1955).
55. Mulliken, R.S. *J. Chem. Phys.*, **36**, 3428 (1962).
56. Ros, P.; Schuit, G. C. A. *Theoret. Chim. Acta*, **4**, 1 (1966).
57. Lever, A. B. P.; Gorelsky, S. I. *Coord. Chem. Rev.*, **208**, 153 (2000).
58. Magnuson, R. H.; Taube, H. *J. Am. Chem. Soc.*, **97**, 5129 (1975).
59. Burdett, J. K. *New J. Chem.*, **21**, 293 (1997).
60. Jung, C.; Ristau, O.; Jung, C. *Theor. Chim. Acta* 1983, **63**, 143 (1997).
61. Sizova, O. V.; Ivanova, N. V.; Ershov, A. Yu.; Nikol'skii, A. B.; Rogachevskii, I. V. *Russ. J. Gen. Chem.*, **67**, 1321 (1997).
62. Sizova, O. V.; Baranovskii, V. I.; Ivanova, N. V.; Nikol'skii, A. B. *Russ. J. Gen. Chem.*, **67**, 1667 (1997).
63. Baranovski, V. I.; Sizova, O. V. *Chem. Phys. Lett.*, **315**, 130 (1999).
64. Ivanova, N. V.; Sizov, V. V.; Nikolskii, A. B.; Panin, A. I. *J. Struct. Chem.*, **40**, 620 (2000).
65. da Cunha, C. J; Fielder, S. S.; Stynes, D. V; Masui, H.; Auburn, P. R.; Lever, A. B. P. *Inorg. Chim. Acta*, **242**, 293 (1996).
66. Shin, Y. K.; Brunschwig, B. S.; Creutz, C.; Newton, M. D.; Sutin, N. *J. Phys. Chem.*, **100**, 1104 (1996).
67. Roothaan, C. C. *J. Rev. Modern Phys.*, **23**, 69 (1951)